Enhancing the activation of silicon carbide tracer particles for PEPT applications using gas-phase deposition of alumina at room temperature and atmospheric pressure

Valdesueiro Gonzalez, D; Garcia-Trinanes, P; Meesters, GMH; Kreutzer, MT; Gargiuli, J; Leadbetter, TW; Parker, DJ; Seville, JPK; van Ommen, JR

DOI
10.1016/j.nima.2015.10.111

Publication date
2016

Document Version
Accepted author manuscript

Published in
Nuclear Instruments & Methods in Physics Research. Section A: Accelerators, Spectrometers, Detectors, and Associated Equipment

Citation (APA)
Valdesueiro Gonzalez, D., Garcia-Trinanes, P., Meesters, GMH., Kreutzer, MT., Gargiuli, J., Leadbetter, TW., Parker, DJ., Seville, JPK., & van Ommen, JR. (2016). Enhancing the activation of silicon carbide tracer particles for PEPT applications using gas-phase deposition of alumina at room temperature and atmospheric pressure. *Nuclear Instruments & Methods in Physics Research. Section A: Accelerators, Spectrometers, Detectors, and Associated Equipment*, *807*, 108-113. https://doi.org/10.1016/j.nima.2015.10.111

Enhancing the activation of silicon carbide tracer particles for PEPT applications using gas-phase deposition of alumina at room temperature and atmospheric pressure

D. Valdesueiro [a], P. Garcia-Trinanes [b, †], G.M.H. Meesters [a], M.T. Kreutzer [a], J. Gargiuli [c], T. Leadbeater [c], D.J. Parker [c], J. Seville [b], J.R. van Ommen [a, †]

[a] Delft University of Technology, Department of Chemical Engineering, 2628 BL Delft, The Netherlands.

[b] Department of Chemical and Process Engineering, Faculty of Engineering and Physical Sciences, University of Surrey, Guildford, Surrey, GU2 7XH, United Kingdom.

[c] Positron Imaging Centre, School of Physics and Astronomy, University of Birmingham, Edgbaston, Birmingham, B15 2TT, United Kingdom.

[†] Email of corresponding authors:

p.garcia@surrey.ac.uk

j.r.vanommen@tudelft.nl

Email of authors:

d.valdesueiro@tudelft.nl

g.m.h.meesters@tudelft.nl

m.t.kreutzer@tudelft.nl

jfgargiuli@gmail.com

t.leadbeater@bham.ac.uk

d.j.parker@bham.ac.uk

j.p.k.seville@surrey.ac.uk

Abstract

We have enhanced the radio-activation efficiency of SiC (silicon carbide) particles, which by nature have a poor affinity towards ^{18}F ions, to be employed as tracers in studies using PEPT (Positron Emission Particle Tracking). The resulting SiC-Al_2O_3 core-shell structure shows a good labelling efficiency, comparable to γ-Al_2O_3 tracer particles, which are commonly used in PEPT. The coating of the SiC particles was carried at 27 ± 3 °C and 1 bar in a fluidized bed reactor, using trimethyl aluminium and water as precursors, by a gas phase technique similar to atomic layer deposition. The thickness of the alumina films, which ranged from 5 to 500 nm, was measured by elemental analysis and confirmed with FIB-TEM (focus ion beam – transmission electron microscope), obtaining consistent results from both techniques. By depositing such a thin film of alumina, properties that influence the hydrodynamic behaviour of the SiC particles, such as size, shape and density, are hardly altered, ensuring that the tracer particle shows the same flow behaviour as the other particles. The paper describes a general method to improve the activation efficiency of materials, which can be applied for the production of tracer particles for many other applications too.

Highlights

- We deposited Al_2O_3 films on SiC particles at ambient conditions in a fluidized bed.
- The affinity of ^{18}F ions towards Al_2O_3-SiC particle was improved compared to SiC.
- We used the Al_2O_3-SiC activated particle as tracer in a PEPT experiment.
- Tracer particles have suitable activity for accurate tracking.
- The Al_2O_3 film is thin enough not to alter the particle size, shape and density.

Keywords

Positron emission particle tracking (PEPT); tracer particle; core-shell particle; atomic layer deposition (ALD); aluminium oxide; fluidized bed reactor.

1. Introduction

Positron Emission Particle Tracking (PEPT) is a powerful non-invasive technique to follow the motion of individual particles in industrial processes [1, 2], which are opaque to other tracking methods [3-5]. The positron emitter most commonly used in such studies is ^{18}F, which has a half-life of 110 minutes. The level of radioactivity of the tracer will define the performance of the PEPT measurement, which depends on the intensity of the signal in the "positron camera" detectors to reconstruct the trajectory of the tracer in the three dimensions [6]. Using a tracer with low emission intensity results in poor resolution of the spatial location of the tracer [7-9].

In previous PEPT studies [10-12], tracers have been produced either by direct irradiation of the sample in a suitable cyclotron, converting oxygen in the sample directly to ^{18}F, or by irradiation of water, which is then exchanged with, or attached to, molecules on the surface of the tracer. The trajectory of the tracer is understood to be representative of the motion of all the particles in the system, which is only the case if the emitting particle is identical, from a granular-matter point of view, to the particles of interest. This can be readily achieved if the particles can adsorb the emitter. However, in some cases this does not occur. This work deals with the problem that appears when the particles do not adsorb the emitter. Then, one can take a different particle to be used as tracer, accepting the mismatch in some properties, or one can develop a particle that emits sufficiently and remains practically identical to the other particles. This paper explores this last option for silicon carbide (SiC) particles.

SiC particles are used as a heat transfer medium in fluidized beds to harvest solar energy in concentrated solar thermal plants [13, 14]. The advantages of SiC in this application include high heat capacity, high sintering temperature, good

77 availability and low cost. The favourable properties of fluidized beds regarding mixing
78 and processability at large scale make them attractive in energy applications such as
79 gasification and combustion of biomass, and chemical looping combustion [15-17]. In
80 all these applications, ensuring and quantifying the good circulation of the particles is
81 essential, and for this PEPT is a uniquely powerful technique. Unfortunately, SiC
82 hardly adsorbs ^{18}F.

83 We demonstrate the production of a core-shell structure to be used as a PEPT
84 tracer particle that better adsorbs the radioactive ions than the core itself. We used SiC
85 as core material and deposited films of Al_2O_3 using a gas-phase coating technique,
86 similar to atomic layer deposition (ALD), using trimethyl aluminium (TMA) and water
87 as precursors, at atmospheric pressure and room temperature [18]. Providing the native
88 SiC particles with a thin coating that can be made radioactive is an attractive
89 alternative to enhance the labelling efficiency of these particles , defined as the ratio of
90 radioactivity absorbed by the SiC particles to the radioactivity of the water solution
91 [19]. Historically aluminium oxide has proved to be a very successful material used for
92 PEPT tracers due to its high affinity for ^{18}F ions [20].

93 The SiC particles used here, with an average particle size ($d_{3,2}$) of 68 μm and
94 density of 3210 kg/m^3 (Appendix A), have the required thermal properties and
95 fluidization behaviour (Geldart A type [21]). However, the inert surface of SiC
96 particles causes poor adsorption of ^{18}F. Other particles with higher labelling
97 performance, such as ion exchange resins or γ-Al_2O_3 particles [22], are effective as
98 emitters, but their different density, size and shape make them poor tracers in this
99 application because their trajectory is different from the SiC particles in the fluidized
100 bed.

ALD is used to deposit inorganic compounds with accurate control based on a set of two reactions repeated a certain number of times [23, 24]. ALD has been applied either to functionalize [25, 26] or protect [27, 28] the surface of flat substrates or powders. We used ALD to reproduce the affinity between ^{18}F ions and the surface of γ-Al_2O_3 particles [20, 22]. Normally, ALD of alumina is performed at about 170°C and absolute pressures of about 1 mbar to ensure the removal of the excess of precursors from the reactor, and obtain atomic growth of the films, i.e. between 0.1 and 0.2 nm per cycle [29-31]. We carried out the coating of SiC particles in a fluidized bed reactor[30, 31] at 1 bar and 27 °C. At these conditions, the removal of the excess of precursors is diminished, and this excess can physisorb on the surface of the SiC particles [32], resulting in a CVD (chemical vapour deposition) type of reaction and thus, higher growth per cycle (GPC) of alumina [18, 33].

To further accelerate the growth of the alumina films, we treated two samples with oxygen plasma prior to coating to increase the initial surface density of hydroxyl groups, crucial to initiate the deposition of alumina (reaction A). The surface of SiC is formed by carbon- and silicon-terminated groups. While carbon-terminated groups are stable and rather inert, silicon-terminated groups are prone to oxidation [34, 35], providing the SiC surface with hydroxyl groups. By using stronger oxidising media, such as oxygen plasma, we can increase the initial density of hydroxyl groups on the surface [36, 37], enhancing the deposition of alumina during the first cycles, achieving higher GPC. Nevertheless, having relatively high GPC is a good compromise between depositing thick films of Al_2O_3 in a fast way, improving the activation with ^{18}F, and preserving the particle properties relevant for the hydrodynamic behaviour of the particles, i.e. size, shape and density.

This experimental paper describes a generic method –using gas phase deposition of alumina– for making tracer particles that closely resemble the original particles. The resulting alumina films are very thin compared to the size of the original particles, and therefore have a negligible influence on properties such as size, shape and density. We demonstrate this with the specific example of the improved labelling efficiency of SiC particles towards ^{18}F ions. For that, we coated five samples of SiC with different thicknesses of Al_2O_3 films, using two deposition temperatures, and surface pre-functionalizing treatment in two of the experiments. After the coating, we radio-activated the five samples with ^{18}F ions, and compared the activity with the uncoated SiC and γ-Al_2O_3 particles. We demonstrate the use of an activated SiC-Al_2O_3 core-shell particle as a tracer in a PEPT experiment on fluidizing SiC particles. Using this novel tracer, more accurate studies on the hydrodynamic behaviour of SiC particles can be performed, increasing knowledge of their behaviour in industrial applications such as direct solar harvesting.

2. Experimental

Al_2O_3 films were deposited in a purpose-built fluidized bed reactor consisting of a glass column of 26 mm in diameter and 500 mm in length. Two stainless-steel distributor plates with pore size of 37 μm, placed at the bottom and top of the column, are used to obtain a homogeneous distribution of the gas inside the column and to prevent particles from leaving the reactor. The reactor and the rest of the setup have been described in detail previously [18, 38]. We use TMA and water as precursors to deposit Al_2O_3 films according to the reaction mechanism (A) and (B). In an ALD process, the surface species in reactions (A) and (B), respectively OH* and CH_3*, determine the completion of the reactions, and once they are depleted, the reactions end. That confers the self-terminating feature to the ALD process, which ensures

atomic growth of the aluminium oxide film. N_2 is pulsed into the reactor in between the reactions for purging purposes. This cycle of reactions can be repeated to grow thicker coatings of aluminium oxide.

(A) $SiC\text{-}OH^* + Al(CH_3)_3 \rightarrow SiC\text{-}O\text{-}Al(CH_3)_2^* + CH_4$

(B) $SiC\text{-}O\text{-}Al(CH_3)_2^* + 2\ H_2O \rightarrow SiC\text{-}O\text{-}Al\text{-}(OH)_2^* + 2\ CH_4$

We calculated the dosing time for TMA based on the maximum amount of TMA molecules that can be accommodated on the surface of the particles [23], considering the steric hindrance between the methyl groups of the TMA, and 0.12 nm as the ligand radius for a TMA molecule [39]. We measured with BET (Brunauer-Emmett-Teller) a specific surface area of 0.12 m^2/g for the SiC particles, and calculated the total particle surface area inside the column for the 8.00 g of powder loaded in the column in each experiment. A N_2 flow of 0.8 L/min, which corresponds to a superficial gas velocity of 2.5 cm/s, was applied to fluidize the powder. To calculate the amount of TMA we dose to the column, we assumed that at the bubbler temperature of 30 °C, TMA is found as dimers [40, 41] and that the components follow the ideal gas law. We estimated, using the model proposed by Mayer *et al*. [42], a saturation of the N_2 bubbles with TMA of about 50%. With these assumptions, we calculated a dosing time of 2.6 seconds for TMA and 2.0 seconds for water to obtain saturation of the particles with the precursors (Appendix B). In order to ensure a faster growth of the alumina films, and therefore, have a higher improvement in the radio-activation of the SiC particles, we overdosed both precursors to the reactor by a factor of about 120 more than the calculated times. With this, we established the dosing times

for the sequence of TMA–N_2–H_2O–N_2, in 5–10–4–10 minutes in all the coating experiments.

We considered that at ambient conditions, the large amount of excess molecules of precursor introduced in each cycle will accumulate on the surface of the particles, resulting in a parasitic-CVD type of growth and thicker films [18]. In addition, we pre-functionalised two samples with oxygen plasma before the coating to obtain a higher GPC. For that, SiC was uniformly spread over a glass Petri dish and introduced into a Harrick Plasma PDC-002 plasma cleaner device for 1 minute; the pressure of the chamber was kept at 6 mbar. Immediately after exposing the SiC to the oxygen plasma, the powder was introduced inside the column to start with the coating experiments.

In total, we performed experiments at five different settings, modifying the number of cycles, operating temperature and pre-functionalization of the SiC particles (Table 1). At 100 °C, we performed two experiments with 5 and 7 cycles. To increase the layer thickness, we lowered the temperature to 27 °C and performed 20 cycles. We carried out the oxygen plasma functionalization, and performed 20 and 40 cycles. In all the experiments we kept constant the initial mass of SiC powder loaded inside the reactor (8.00 g), the flow of nitrogen (0.8 L/min), and dosing times of the precursors and purging N_2 (5–10–4–10 minutes).

To characterize the coating process, we calculated the thickness of the alumina films (δ_{ICP}) from the elemental analysis of the samples carried out with a Perkin Elmer Optima 500 ICP-OES (Induced Coupled Plasma – Optical Emission Spectroscopy). We obtain the mass fraction of aluminium (x_{Al}) from ICP, from which we calculate the thickness of the alumina coating [18]. For this calculation, we used a density for the SiC particles of 3210 kg/m^3, and for alumina of 2500 kg/m^3 [43]. We measured a mass fraction of aluminium of 0.0007 in the uncoated SiC particles, and used this value to

199 correct the fraction of aluminium in the coated samples, to consider only the
200 aluminium deposited as Al_2O_3 in the calculation of the film thickness. To compare the
201 thickness calculated from elemental analysis, we measured the thickness directly from
202 a TEM (Transmission Electron Microscope) image for the sample with 40 cycles. For
203 that, we produced a lamella in the nanometre range of the coated SiC using FIB
204 (Focused Ion Beam) [44] combined with TEM.
205 Extending the earlier discussion, radio-activation of the tracer can be achieved
206 according to three different techniques: *direct activation*, *ion exchange* and *surface*
207 *modification* [7, 45]. In this work, we used a procedure similar to the ion exchange
208 method, using ^{18}F as radioactive source [6]. To activate the particles we prepared an
209 extremely dilute solution of ^{18}F ions in pure water produced by bombardment with an
210 energetic ^{3}He beam from the Birmingham MC40 cyclotron. Oxygen atoms within the
211 solution are converted into ^{18}F ions in the two competing reactions described by Fan *et*
212 *al* [7]. A sample of our coated particles was immersed into the solution for around one
213 hour allowing contact between ^{18}F ions and the Al_2O_3 surface layer of the coated SiC
214 particles. The liquid was evaporated and the particles dried, thus allowing their
215 recovery and subsequent measurement. The activity of the samples was measured with
216 a *CRC-15R Capintenc Inc.* radioisotope calibrator [45]. To compare the activation of
217 the different SiC samples and the γ-Al_2O_3, we calculated the relative activity as the
218 ratio of the activity of the particles, with a value in the μCi range, and the activity of
219 the radioactive solution, in the mCi range. Finally, to confirm the applicability of the
220 tracer particle produced, we used one radio-activated particle of the SiC sample coated
221 for 40 cycles with aluminium oxide to perform a PEPT experiment in a fluidized bed.
222 We fluidized SiC for 30minutes in a column of 90mm in diameter and 500mm in

length, and reconstructed the trajectory of the tracer particle based on the triplets $(\bar{x}, \bar{y}, \bar{z})$ measured by the ADAC "positron camera" [2].

3. Results and discussion

Table 1 shows the experiments carried out with different numbers of coating cycles (5, 7, 20 and 40 cycles), different reaction temperatures (100 and 27 °C) and pre-functionalization of the powder with O_2 plasma. As we expected, the mass fraction of aluminium (x_{Al}) and, therefore, the thickness of the alumina films (δ_{ICP}) increased with: (i) an increasing number of cycles, (ii) a decrease in the reaction temperature, and (iii) the pre-functionalization of the SiC particles (Table 1). We obtained a GPC of 1-2 nm for the experiments at 100 °C, which is calculated after dividing the thickness of the alumina film over the number of cycles. When reducing the temperature to 27 °C we achieved a GPC of 9 nm after 20 cycles. This shows the influence of the temperature on the accumulation of unreacted precursor molecules. In addition, we observed an increase in the GPC after the functionalization of the SiC particles with O_2 plasma for the experiment with 20 cycles. That can be explained by an increase of the surface density of hydroxyl groups during the plasma treatment, which will promote a larger deposition during the initial cycles of the experiment. We obtained a GPC from 1 to 12 nm in the different experiments, which is much larger than the characteristic GPC for ALD, typically 0.1-0.2 nm [18, 46-49]. This is due to the long dosing times of both precursors, far beyond the dosage to fully saturate the surface of the particles. At 27 °C, the molecules of the precursors in excess accumulate on the surface, losing the self-terminating feature of the ALD reactions, and inducing higher GPC [18]. Based on the GPC, these experiments cannot be considered as ALD. However, neither do the GPC values in this work indicate a typical CVD mechanism, where the precursors are dosed simultaneously to the reactor, and films grow with rates around 0.1 μm/min for

248 similar metal oxides [50], nor as Rapid ALD process [51], where the precursors acts as
249 catalyst to deposit layers of about 2 nm per cycle.

250 To validate the thickness calculated from the elemental analysis, we measured
251 the thickness of the Al_2O_3 film of the sample coated for 40 cycles using FIB combined
252 with TEM and EDX (Fig. 1 and Appendix C and D). To prepare a lamella with FIB,
253 we first deposited a protective layer of platinum of about 100 nm to avoid damaging
254 the alumina film during the bombardment of ions (Appendix C). We placed the lamella
255 under the TEM, and measured a film thickness of about 400 nm (Fig. 1) after
256 measuring the thickness at 50 points taken from two TEM images. This result is
257 comparable to the one calculated from elemental analysis, 484 ± 52 nm (Table 1).

258 In Fig. 1, lighter areas in the alumina film are visible. These might be air
259 pockets or pores in the film. We verified the porosity of the alumina film of the sample
260 coated for 40 cycles of Al_2O_3 with BET measurements (Appendix E). The specific
261 surface area measured for the uncoated SiC particles, 0.12 m^2/g, is near the detection
262 limit. The larger diameter of the coated sample produces a decrease in the BET surface
263 area, falling below the detection limit of the measuring device (Appendix E). That can
264 be seen by the shape of the BET isotherms for the coated sample, which is similar to
265 that for an empty measuring probe. Nevertheless, the pores seen in Fig. 1 would have
266 produced a strong increase of the surface area, especially since we are working near the
267 detection limit. It might be that these non-homogeneities found in the alumina film
268 (Fig. 1) are either inaccessible to the nitrogen during the BET measurement, or
269 produced during the sample preparation with FIB. In any case, these cannot be
270 measured with nitrogen adsorption.

271 Fig. 2a shows the activity of the samples relative to the activity of the
272 radioactive water used in the activation, expressed as a percentage. Between the

uncoated sample (0.009%) and the γ-Al_2O_3 (0.143%), we observed an increase in the relative activity with the thickness of the alumina film. The samples with the thin coating (5 and 7 cycles) showed a slight improvement with regard to the uncoated SiC. The experiment with 20 cycles of Al_2O_3 at 27 °C showed a strong improvement of the activity, which was further increased when the SiC particles were pre-functionalized with the oxygen plasma. The sample with 40 cycles at 27 °C, and O_2 plasma pre-treatment showed the best relative activity, 0.108%. As we expected, the efficiency of the radio-activation increased with the thickness of the alumina films (Fig. 2b). The sample with 40 cycles shows a relative activity comparable to the one of γ-Al_2O_3, often used as tracer.

To evaluate the properties of the SiC sample coated with 40 cycles, we calculated an equivalent density of the core-shell particle using (Eq. 1) and compared the value to the uncoated SiC (Table 2). For that, we defined the core-shell density ($\rho_{core-shell}$) as a weighted average considering the volume fractions of SiC (φ_{SiC}) and the alumina coating (φ_{Al2O3}).

$$\rho_{core-shell} = \frac{d_P^3}{(d_P+2\cdot\delta_{Al2O3})^3}\cdot\rho_{SiC} + \frac{(d_P+2\cdot\delta_{Al2O3})^3-d_P^3}{(d_P+2\cdot\delta_{Al2O3})^3}\cdot\rho_{Al2O3} \qquad \text{Eq. (1)}$$

We calculated the density of the core-shell for the 40-cycle sample, since it showed the thickest alumina film and the highest relative activity with ^{18}F. For this sample, an alumina film of 484nm corresponds to a volume fraction of alumina (φ_{Al2O3}) of 0.03. Considering the density of SiC of 3210 kg/m^3, and the density of Al_2O_3 deposited with ALD at room temperature of 2500 kg/m^3 [43], we obtained a density of the core-shell of 3180 kg/m^3. This represents a density difference of 0.8% with respect to the uncoated SiC (Table 2), which is a negligible difference as far as the

298 particle dynamic behaviour is concerned. Moreover, we consider that neither the size
299 nor the shape of the SiC particles substantially changed with the alumina film, since
300 the thickness of the alumina film is much smaller than the particle diameter. Therefore,
301 we can conclude that the deposited alumina film does not alter the density, shape and
302 size of the SiC particles, which are the most relevant properties for the hydrodynamic
303 behaviour of fluidizing particles.

304 We used a radio-activated particle of the SiC sample coated with Al_2O_3 during
305 40 cycles to perform a PEPT experiment. During the 30 minutes that the experiment
306 lasted, we obtained over 17000 x,y,z locations in time (Fig. 3), which translates to an
307 average sampling frequency of about 10 Hz. The size of the tracer will affect the
308 activity, which influences the sampling data, and eventually may affect the precision of
309 the PEPT reconstruction; i.e. smaller particles result in lower activities which result in
310 lower spatial resolution [19].

311 In this work, we used as tracer the same 68 μm particles as in the rest of the bed,
312 coated with 40 cycles of aluminium oxide. The corresponding average activity was 22
313 μCi which allowed accurate measurement of the position of the tracer at a frequency of
314 10 Hz. The bare SiC particles, with an activity of 2 μCi, would have allowed only
315 measurements at a lower frequency (~1 Hz). The most relevant dynamics in fluidized
316 beds take place in the frequency range 0-6 Hz based on pressure fluctuations [52], or
317 even the lower part of that range based on solids motion. In the case of the experiment
318 with the 40-cycle SiC, we found that the power spectrum has little powder above 2 Hz,
319 such as sampling at 10 Hz is sufficient to capture all the dynamics, while sampling at 1
320 Hz would certainly miss relevant dynamics.

321 In Fig. 3a we see the trajectory of the tracer during the first 10 seconds of
322 fluidization. We observed that the intensity of the SiC sample coated with 40 cycles

provides sufficient data points for the PEPT algorithm to be applied and for description of the location and movement of the tracer. In Fig. 3b, we show all the data points recorded during the 30 minutes of the experiment. The projections of the data points on the different planes give an idea of the uniform spread of the measured locations inside the fluidized bed, illustrating that tracking was possible throughout the measurement volume. Fig. 3c shows the mobility of the tracer in each of the three axes over a duration of 200 seconds. During the first 20 seconds of the measurement (Fig. 3c), there was no fluidization and the tracer rested almost at the bottom of the bed of particles, and once the fluidization began, the tracer started moving inside the bed.

Despite the lower activity and sampling frequency for the alumina-coated SiC tracer when compared to other tracers, the coating method used here allowed us to track and reconstruct the 3D trajectory of a SiC particle, which would have been impossible without the alumina coating. This generic approach could be extended to other types of applications where a tracer particle is needed, such as PEPT or RPT (Radioactive Particle Tracking).

4. Conclusions

We demonstrated that initially inert particles, such as SiC, can be activated with ^{18}F ions by modifying the surface of the primary SiC particles. For that, we deposited aluminium oxide films on the SiC particles in a fluidized reactor using a gas-phase coating technique similar to atomic layer deposition. Contrary to conventional ALD, we carried out coating at atmospheric pressure and room temperature. At these conditions, we fed the precursors in large excess to ensure a fast growth of the alumina films. On the sample coated for 40 cycles, which was pre-functionalized with O_2 plasma, we deposited a film of about 500 nm, resulting in a GPC of about 12 nm. This 40-cycles coated sample presented a labelling efficiency with ^{18}F similar to that for the

348 γ-Al_2O_3, which is often used as a tracer. We conclude that the layer is thick enough to
349 enable sufficient activity, yet thin enough to make the changes in density, size and
350 shape of the particles negligible.
351 We showed that the activated core-shell structure formed by the SiC particle
352 coated with an Al_2O_3 film of about 500 nm can be used as a tracer particle in a typical
353 PEPT experiment. The emission intensity of this tracer was sufficient to reconstruct its
354 trajectory inside the bed of particles albeit at suboptimal performance (i.e. low location
355 rate and corresponding lower precision than generally quoted for PEPT). That proves
356 that the deposition of alumina films can be used to produce tracers, mainly consisting
357 of the same material as the bulk. This will enable researchers to obtain more accurate
358 information about the flow patterns in systems with moving particles.
359
360 **5. Author contributions**
361 D.V. performed the coating experiments, and P.G.T, J.G and T.L. carried out the
362 activation of the tracers and the PEPT experiments. All the authors were involved in
363 the discussion of the results. The manuscript was prepared by D.V., and revised by the
364 rest of the authors. All authors give approval to the final version of the manuscript.
365
366 **6. Acknowledgements**
367 We would like to acknowledge the Department of Chemical and Environmental
368 Engineering and Aragón Nanoscience Institute in Zaragoza (Spain), and in particular
369 Prof. Dr. Jesús Santamaría, Dr. Francisco Balas and Alberto Clemente for the
370 preparation and analysis of the samples with the FIB-TEM. D.V., G.M.H.M., M.T.K.
371 and J.R.vO. were supported financially by the European Union Seventh Framework
372 Program FP7/2007-2013 under grant agreement no. 264722. D.V., G.M.H.M., M.T.K.

and J.R.vO. acknowledge Royal DSM for partly funding this research. P.G.T., J.G., T.L., D.J.P. and J.S. acknowledge the European Commission for co-funding the CSP2 Project Concentrated Solar Powder in Particles (FP7, Project 282932).

7. References

[1] D.J. Parker, C.J. Broadbent, P. Fowles, M.R. Hawkesworth, P. McNeil, Nuclear Instruments and Methods in Physics Research Section A: Accelerators, Spectrometers, Detectors and Associated Equipment 326/3 (1993) 592.

[2] D.J. Parker, R.N. Forster, P. Fowles, P.S. Takhar, Nuclear Instruments and Methods in Physics Research Section A: Accelerators, Spectrometers, Detectors and Associated Equipment 477/1–3 (2002) 540.

[3] J.P.K. Seville, A. Ingram, D.J. Parker, Chemical Engineering Research and Design 83/7 A (2005) 788.

[4] A.C. Hoffmann, C. Dechsiri, F. Van De Wiel, H.G. Dehling, Measurement Science and Technology 16/3 (2005) 851.

[5] J. Chaouki, F. Larachi, M.P. Duduković, Industrial and Engineering Chemistry Research 36/11 (1997) 4476.

[6] D.J. Parker, X. Fan, Particuology 6/1 (2008) 16.

[7] X. Fan, D.J. Parker, M.D. Smith, Nuclear Instruments and Methods in Physics Research Section A: Accelerators, Spectrometers, Detectors and Associated Equipment 562/1 (2006) 345.

[8] T.S. Volkwyn, A. Buffler, I. Govender, J.P. Franzidis, A.J. Morrison, A. Odo, N.P. van der Meulen, C. Vermeulen, Minerals Engineering 24/3–4 (2011) 261.

[9] M. Bickell, A. Buffler, I. Govender, D.J. Parker, Nuclear Instruments and Methods in Physics Research Section A: Accelerators, Spectrometers, Detectors and Associated Equipment 682/0 (2012) 36.

[10] D. Boucher, Z. Deng, T. Leadbeater, R. Langlois, M. Renaud, K.E. Waters, Minerals Engineering 62/0 (2014) 120.

403 [11] C.W. Chan, A. Brems, S. Mahmoudi, J. Baeyens, J. Seville, D. Parker, T.
404 Leadbeater, J. Gargiuli, Particuology 8/6 (2010) 623.
405 [12] C.W. Chan, J. Seville, X. Fan, J. Baeyens, Powder Technology 194/1-2 (2009)
406 58.
407 [13] G. Flamant, D. Gauthier, H. Benoit, J.L. Sans, R. Garcia, B. Boissière, R.
408 Ansart, M. Hemati, Chem. Eng. Sci. 102 (2013) 567.
409 [14] G. Flamant, D. Gauthier, H. Benoit, J.L. Sans, B. Boissière, R. Ansart, M.
410 Hemati, Energy Procedia 49/0 (2014) 617.
411 [15] D. Kunii, O. Levenspiel, Fluidization Engineering, Butterworth-Heinemann,
412 1991.
413 [16] A. Lyngfelt, B. Leckner, T. Mattisson, Chem. Eng. Sci. 56/10 (2001) 3101.
414 [17] W. Zhong, B. Jin, Y. Zhang, X. Wang, R. Xiao, Energy & Fuels 22/6 (2008)
415 4170.
416 [18] D. Valdesueiro, G. Meesters, M. Kreutzer, J. van Ommen, Materials 8/3 (2015)
417 1249.
418 [19] K.E. Cole, A. Buffler, N.P. van der Meulen, J.J. Cilliers, J.P. Franzidis, I.
419 Govender, C. Liu, M.R. van Heerden, Chem. Eng. Sci. 75 (2012) 235.
420 [20] B. Kasprzyk-Hordern, Advances in Colloid and Interface Science 110/1–2
421 (2004) 19.
422 [21] D. Geldart, Powder Technology 7/5 (1973) 285.
423 [22] X. Fan, D.J. Parker, M.D. Smith, Water Research 37/20 (2003) 4929.
424 [23] R.L. Puurunen, Chemical Vapor Deposition 9/5 (2003) 249.
425 [24] S.M. George, Chem. Rev. 110/1 (2010) 111.
426 [25] A. Goulas, J. Ruud van Ommen, Journal of Materials Chemistry A 1/15 (2013)
427 4647.

[26] S.D. Elliott, Langmuir 26/12 (2010) 9179.

[27] B. Moghtaderi, I. Shames, E. Doroodchi, Chemical Engineering and Technology 29/1 (2006) 97.

[28] D.M. King, X. Liang, B.B. Burton, M. Kamal Akhtar, A.W. Weimer, Nanotechnology 19/25 (2008).

[29] J.R. Wank, S.M. George, A.W. Weimer, Journal of the American Ceramic Society 87/4 (2004) 762.

[30] L.F. Hakim, J. Blackson, S.M. George, A.W. Weimer, Chemical Vapor Deposition 11/10 (2005) 420.

[31] D.M. King, J.A. Spencer Ii, X. Liang, L.F. Hakim, A.W. Weimer, Surface and Coatings Technology 201/22-23 SPEC. ISS. (2007) 9163.

[32] S. Salameh, J. Schneider, J. Laube, A. Alessandrini, P. Facci, J.W. Seo, L.C. Ciacchi, L. Mädler, Langmuir 28/31 (2012) 11457.

[33] S.M. George, A.W. Ott, J.W. Klaus, Journal of Physical Chemistry 100/31 (1996) 13121.

[34] R.P. Socha, K. Laajalehto, P. Nowak, Colloids and Surfaces A: Physicochemical and Engineering Aspects 208/1–3 (2002) 267.

[35] G. Cicero, A. Catellani, G. Galli, Physical Review Letters 93/1 (2004) 016102.

[36] J.R. Hollahan, G.L. Carlson, Journal of Applied Polymer Science 14/10 (1970) 2499.

[37] M. Morra, E. Occhiello, F. Garbassi, Langmuir 5/3 (1989) 872.

[38] R. Beetstra, U. Lafont, J. Nijenhuis, E.M. Kelder, J.R. Van Ommen, Chemical Vapor Deposition 15/7-9 (2009) 227.

[39] V. Dwivedi, R.A. Adomaitis, 17th International Chemical Vapor Deposition Symposium (CVD-XVII) - 216th Meeting of the Electrochemical Society, Vienna, 2009, p. 115.

[40] C.H. Henrickson, D.P. Eyman, Inorganic Chemistry 6/8 (1967) 1461.

[41] A.W. Laubengayer, W.F. Gilliam, Journal of the American Chemical Society 63/2 (1941) 477.

[42] B. Mayer, C.C. Collins, M. Walton, Journal of Vacuum Science & Technology A 19/1 (2001) 329.

[43] M.D. Groner, F.H. Fabreguette, J.W. Elam, S.M. George, Chemistry of Materials 16/4 (2004) 639.

[44] R. Wirth, Chemical Geology 261/3–4 (2009) 217.

[45] X. Fan, D.J. Parker, M.D. Smith, Nuclear Instruments and Methods in Physics Research, Section A: Accelerators, Spectrometers, Detectors and Associated Equipment 558/2 (2006) 542.

[46] L.F. Hakim, J.L. Portman, M.D. Casper, A.W. Weimer, Austin, TX, 2004, p. 2339.

[47] J.R. Wank, L.F. Hakim, S.M. George, A.W. Weimer, Fluidization XI - Present and Future of Fluidization Engineering, ECI International (Brooklyn, NY). U. Arena, R. Chirone, Ml. Miccio, and P. Salatino, editors. p. 603-610 (2004) 8.

[48] J.D. Ferguson, A.W. Weimer, S.M. George, Thin Solid Films 371/1 (2000) 95.

[49] L.F. Hakim, J.A. McCormick, G.D. Zhan, A.W. Weimer, P. Li, S.M. George, Journal of the American Ceramic Society 89/10 (2006) 3070.

[50] K. Fujino, Y. Nishimoto, N. Tokumasu, K. Maeda, Journal of the Electrochemical Society 137/9 (1990) 2883.

[51] D. Hausmann, J. Becker, S. Wang, R.G. Gordon, Science 298/5592 (2002) 402.

476 [52] J.R. van Ommen, R.-J. de Korte, C.M. van den Bleek, Chemical Engineering
477 and Processing: Process Intensification 43/10 (2004) 1329.
478
479
480

8. List of figures

9. List of tables

Figures and Tables

Table 1. Mass fraction of aluminium, determined by ICP, and the thickness of the alumina film, calculated from the results from ICP, for the different experiments.

# cycles	O_2 Plasma	T [°C]	x_{Al} [-]	δ_{ICP} [nm]	GPC [-]
5		100	0.02	5.5 ± 0.6	1.1 ± 0.1
7		100	0.06	16.5 ± 1.7	2.4 ± 0.2
20		27	0.67	183.2 ± 19.4	9.2 ± 1.0
20	●	27	0.84	229.4 ± 24.3	11.5 ± 1.2
40	●	27	1.79	484.2 ± 52.3	12.1 ± 1.3

Table 2. Density comparison between the uncoated SiC and the sample coated with 40 cycles.

	SiC	Al_2O_3-SiC
d [µm]	68	68.8
δ_{Al2O3} [µm]	-	0.4
φ_{SiC} [-]	1	0.97
φ_{Al2O3} [-]	0	0.03
ρ [kg/m^3]	3210	3185

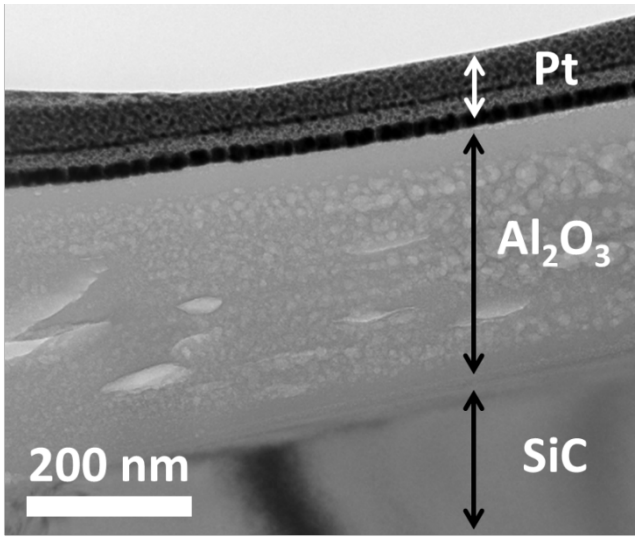

Figure 1. FIB-TEM image of the SiC sample coated for 40 cyclesof Al_2O_3. The film thickness is about 400nm.

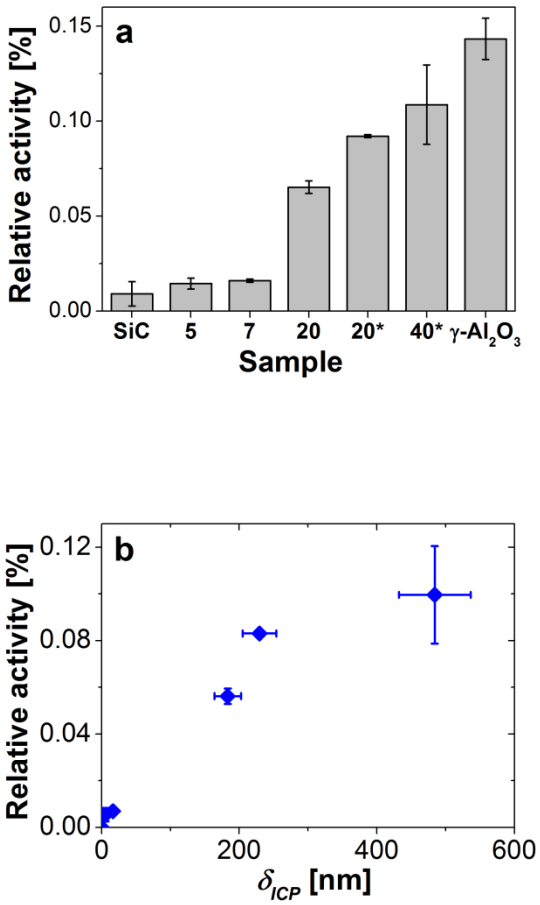

505

506 **Figure 2. (a)** Relative activity, in percentage, of the uncoated SiC, coated samples and
507 the γ-Al_2O_3 sample. **(b)** Relative activity of the coated samples with respect to the film
508 thickness. In both pictures, the vertical error bars represent the standard deviation of
509 the activity measurements over the square root of the number of measurements. The
510 horizontal error bars in Fig. 2b represent the error introduced in the calculation of the
511 film thickness, based on the error of the ICP-OES equipment and the density of the
512 alumina film.

513

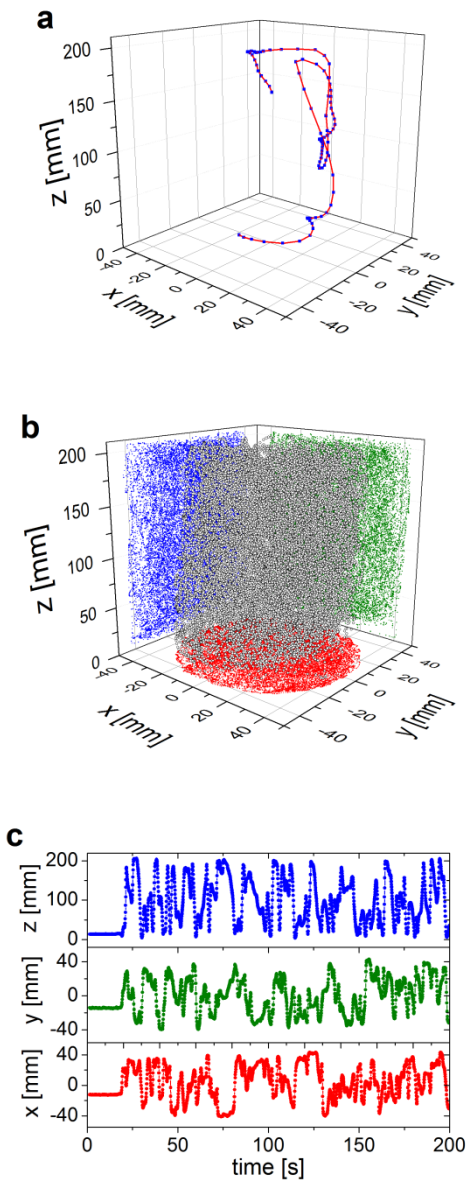

514

515 **Figure 3. (a)** 3D representation of the trajectory of the SiC-Al_2O_3 tracer during the 10 first
516 seconds of fluidization in the PEPT experiment. **(b)** Representation of all the data points
517 during the 30 minutes of the PEPT experiment. The projections of the data in each of the
518 planes are shown with red, green and blue symbols. **(c)** Mobility of the tracer in each of the
519 axes during the first 200 seconds of the PEPT experiments. Within this 200 second period, in
520 the first 20 seconds there is no fluidization, so that the tracer remained stationary near the
521 bottom of the bed of particles.

522

523